CHAPTER-3

3.1.Introduction

In this chapter, application of Ba-La mixed metal oxide as heterogeneous base catalyst is emphasized for methyl ester production from *Madhuca longifolia* oil feedstock using transesterification reaction. The Ba-La mixed metal oxide, a novel catalyst was synthesized by four different methods i.e., co-precipitation (BLOC), solid state (BLOS) and sol-gel autocombustion method (also known as citrate route) (BLOA1 and BLOA2). The catalyst samples were characterized by sophisticated methods and their catalytic activity was measured by quantifying the FAME content of the biodiesel. The fatty acid profile of feedstock was analyzed by GC-MS. It has been observed that BLOA1, BLOA2, and BLOC resemble with each other as they have one phase common in all with an identical structural formula of $Ba_2La_2O_5$. This observed structural formula constituted the mixture of the spinel and metal oxides. The BLOS sample had the structural formula of $Ba_{10}La_2O_{13}$ which proved the extensive formation of individual metal oxides. Out of the samples, BLOA2 synthesized by citrate route was efficient in methyl ester production. The citrate route synthesis performed at pH 2.31 enriched the catalyst mixed metal oxide surface with free OH^- groups, which ultimately avoided formation of the carbonate species, produced biodiesel with 97.2±0.5% FAME conversion. Hence, Ba-La mixed metal oxide prepared by citrate route in acidic medium is a potential catalyst for biodiesel production via transesterification. The kinetic experiments of transesterification reaction approved that reaction mechanism followed first order kinetics with activation energy (E_A) of 34.44kJmol^{-1}. The thermodynamic functions such as ΔH°, ΔS°, and ΔG° and were also

determined and found to be 32.12 kJ/mol, -188.33 J/mol, and 95.78 kJ/mol at 65˚C. The positive value of Gibbs free energy (ΔG˚) suggested the transesterification reaction as non-spontaneous or external force driven reaction which validates the need of heterogeneous catalysis. The E-factor and turn over frequency (TOF) were also determined and found to be 0.089 and 23×10^{-2} s^{-1}. The physicochemical properties of the synthesized fatty acid methyl esters (FAME) were measured according to ASTM D 6751 and were found to be within the permissible range.

3.2. Catalyst synthesis

In order to explore the effect of synthesis route exactly on FAME production, catalyst was synthesized by four different methods and analyzed for its catalytic activity for biodiesel production.

3.2.1. Sol-gel auto combustion method

Barium lanthanum mixed metal oxide was synthesized by sol-gel auto combustion method. Two samples namely BLOA1 and BLOA2 were synthesized by this method. To synthesize BLOA1, the analytical grade $Ba(NO_3)_2$, $La(NO_3)_3$, and Citric acid were used as starting materials. Nitrate precursors of raw material with stipulated molar ratio Ba/La along with an equimolar amount of citric acid as a complexing agent were dissolved in distilled water. Nitrate-citrate salt was stabilized through dropwise addition of 25% ammonia solution till pH 7. The solution was stirred continuously at 60˚C which resulted in formation of nitrate-citrate salt. Afterwards, sol was heated slowly to 130˚C causing evaporation of excess water. Further, it was kept for continued heating at 350˚C. This caused further removal of volatile carbonaceous matter resulting in gradual change in viscosity as well as color. The continuous heating

formed a brown fluffy porous dry gel which further got automatically ignited owing to thermally induced oxidation-reduction reaction. Finally, the solid oxide powder was obtained by auto-ignition method. The uncalcined material was examined through TGA/DTA. From thermal analysis, stable phase of the catalyst was obtained at 800°C. Therefore, solid oxide powder was calcined in a muffle furnace at 800°C for 4h with a heating rate of 10°C/min. The synthesized sample was ground with the help of agate mortar and sieved to obtain fine powder before it was used as a catalyst. The second sample (BLOA2) was prepared just adopting the same procedure as in above case, except the addition of ammonia solution to stabilize the nitrate-citrate salt. During the sample preparation, no precipitation or turbidity was observed, and solution remained approximately pH 2, extremely acidic medium.

3.2.2. Co-precipitation method

Co-precipitation route was adopted for the synthesis of Ba-La mixed metal oxide (BLOC). The procedure adopted for catalyst preparation was as follows. Nitrate precursors of barium and lanthanum were taken in a definite stoichiometric ratio and were dissolved in distilled water having the final concentration of 0.6M. The precipitation occurred by dropwise addition of equimolar sodium carbonate solution till the final pH of 10 with continuous agitation. The precipitated material was separated from its mother liquor using Whatman filter paper followed by extensive washing with distilled water to de-contaminate it from nitrate ion and then, dried in an oven at 80°C overnight. Further, mixed metal hydroxide powder was calcined in a muffle furnace at 800°C for 4h with a heating rate of 10°C/min.

3.2.3. Solid state route

The BLOS catalyst was synthesized by solid-state method. In this technique, nitrate precursors were taken in a fixed stoichiometric ratio. Starting materials were ball milled for 7h with acetone as binding agent. The crude catalyst underwent for calcination at 800˚C for 4h. Finally, the prepared catalyst was placed in a desiccator for further application.

3.3. Catalyst characterization

The samples (BLOA1, BLOA2, BLOC and BLOS) synthesized by the different experimental procedures exhibited distinct structures, chemical compositions, and catalytic activities. The most important parameter used to evaluate the catalytic activity in a transesterification reaction is the FAME conversion. To evaluate the catalytic strength, the samples were characterized and their results are described in the upcoming sections based on the catalytic conversion values.

3.3.1. Thermal analysis

Figure 3.1 shows the thermo-gravimetric curves which depict the thermal behavior of catalysts comprising multiple decomposition steps. The first behavior, observed for samples prepared by the co-precipitation and solid-state methods included two similar consecutive mass loss i.e. BLOS had suffered 2.7% and 8.3% mass loss while BLOC underwent for 3.01% and 7.8% mass loss subsequently. These two sharp losses in both cases occurred in two temperature zones i.e., 40˚C-400˚C and 600˚C-750˚C which further attributed to loss of water and degradation of nitrate precursor along with the evolution of CO_2 as a result of carbonate species degradation respectively.

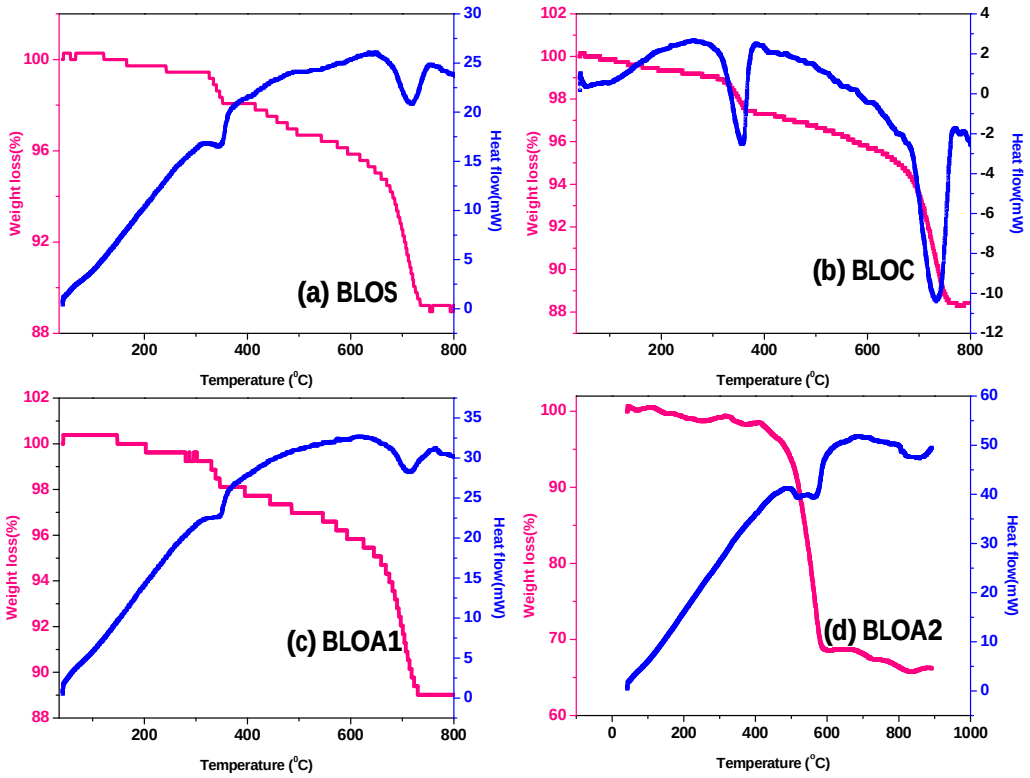

Figure 3.1 Thermal curves of catalysts prepared by different synthesis routes: (a) BLOS, (b) BLOC, (c) BLOA1, (d) BLOA2.

But, there was a sharp mass loss because at each stage major mass loss was simultaneously assisted by water and residual compound losses, as well as structure changes that consolidate d the mixture of the different metal oxides, according to the XRD analysis. A second decomposition profile was observed in the citrate route samples (Figure 3.1). Despite having almost the same synthesis route, the catalysts followed different patterns of mass losses by an order of magnitude. In case of citrate route, BLOA1 and BLOA2 suffered one and two mass losses respectively. BLOA1, the very first and almost negligible mass loss was recorded in the range of 200˚C-350˚C and it was attributed to the loss of water and some organic compounds due to residual citric acid. The major loss was roughly 11.1% for BLOA1 and 10.9% for BLOA2 in 400˚C-750˚C temperature range in both cases at the degradation of organic moieties

and nitrate precursors along with carbonate species and structural hydroxyl group losses. In general, the alkaline pH used in co-precipitation route favored metal oxide formation in the native form, i.e., pure barium oxide, lanthanum oxide, and the mixed perovskite seemed to be dependent on controlled atoms diffusion during the reaction. This atomic diffusion was enhanced while citrate route was adopted (Yue et al., 2000). Furthermore, the formation of the M-citrate complex responsible for metal diffusion control was more efficient at the neutral pH condition (Jaimeewong et al., 2016). In citrate route, aside from favoring the perovskite structure, the experimental conditions were more effective at controlling the oxide surface composition, leading to the preferential formation of the oxo-bond (M-O-M) (Jaimeewong et al., 2016). The oxo-groups on the oxide surface were less susceptible to the hydrolysis than the other more reactive surface groups, and they reacted to carbon dioxide molecules to produce a surface rich in carbonate species. The sample synthesized under acidic pH conditions (BLOA2) had more surface hydroxyl groups due to high concentration of hydrogen ions in the reaction medium that favored hydrolysis reaction (Limaa et al., 2012). Then, the highly hydroxylated surface was stabilized by water adsorption molecules instead of atmospheric CO_2 adsorption. It avoided the surface poisoning by atmospheric CO_2 and resulted only mixed metal oxide formation. Since all the four TGA curves belonging to four catalyst samples suggested the optimum calcination at 800˚C, crude catalysts were subjected to calcination at 800˚C for 4h.

3.3.2. Powder XRD analysis

The following diffractogram shows prominent peaks regarding prepared catalysts demonstrating the phase and structural unit cell parameters. Figure 3.2 (a, b, c, & d) represent diffractogram of catalysts synthesized through different routes such as

sol-gel auto-combustion, co-precipitation, and solid state, respectively.

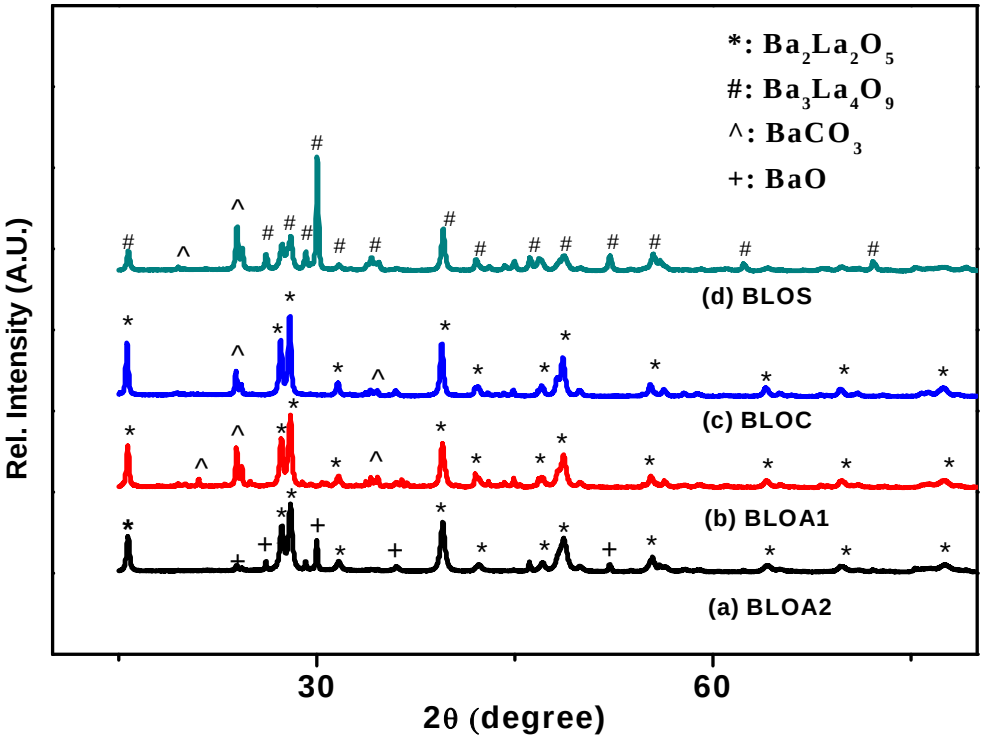

Figure 3.2 X-ray diffractogram of calcined catalysts at 800˚C: (a) BLOA2, (b) BLOA1, (c) BLOC, and (d) BLOS.

Interestingly, former two synthesis routes incorporate a quite similar phase and structural geometry in catalyst substantiated by the results obtained in Figure 3.2 (a & b). This may be attributed to the analogous way of crystal formation during precipitation and formation of sol succeeded by gelation. As crystal formation involves two subsequent steps i.e., nucleation and growth (Driessche et al., 2017), it brought this aforementioned similarity in catalyst phases prepared by citrate route and co-precipitation route. The structure and geometrical formula of the catalyst was predicted after matching with JCPDS file. In diffractogram Figure 3.2 (a, b, and c), four major peaks with prominent intensity diffracted at 15.7˚, 28˚, 39.6˚ and 48.8˚ got matched with JCPDS file no#521325 which depicts the structural formula as $Ba_2La_2O_5$ and

informed about the crystal structure of catalyst as regular orthorhombic. The samples with this structural formula constitute a mixture of barium oxide (BaO) and spinel ($BaLa_2O_4$). As there is less significant size difference between barium and lanthanum, the complete formation of spinel was not feasible here. In addition to peaks as mentioned above in Figure 3.2 (b and c), high-intensity peaks at 24.09˚(111), and 34.15˚(112) resembled with JCPDS file #712394 showing the presence of $BaCO_3$ along with $Ba_2La_2O_5$ within lattice stoichiometry. But, in case of Figure 3.2(a) which represents the diffractogram with high-intensity peaks corresponding to $Ba_2La_2O_5$ exclusively with no additional peaks of $BaCO_3$. That's why sample BLOA2 showed the best activity. In case of BLOA1 sample, barium oxide showed philicity towards CO_2 which is reflected regarding $BaCO_3$ shown by XRD Diffractogram in Figure 3.2(b). Sample BLOC also showed some minute extent of metal carbonate significantly because of carbonate containing precipitating agent. At alkaline pH, prepared naked metal oxides are susceptible for metal carbonate formation which is further supported by XRD diffractogram as in Figure 3.2(b). That's why its activity gets hampered in transesterification reaction for biodiesel production. In BLOA1 sample, oxo bond (M-O-M) is more susceptible to CO_2 to make surface rich with $BaCO_3$ rather than hydrolysis reaction to increase basicity of prepared catalyst. But BLOA2 sample was capable of avoiding this problem because metal oxide formation at acidic pH led to the richness of surface with hydroxyl group because of excess H^+ concentration in reaction media. As a result of this phenomenon, sample BLOA2 lacked the presence of carbonate species. This kept catalyst intact in the form of oxide which actively participates as a catalyst in transesterification reaction. Notwithstanding, catalyst prepared by solid state route seeks more attention as it upholds entirely different crystal

structure and structural formula. On comparing with JCPDS file no #521326, the catalyst was confirmed to bear same crystal structure but with different empirical formula as $Ba_{10}La_2O_{13}$. The major problem which occurs with solid state route is the requirement of higher temperature in comparison to former synthesis routes. Here, the insertion of both elements in lattice array is not quiet prominent because the stronger intermolecular interactions in native oxide forms. Hence, it avoids the spinel formation in crystal lattice which is probably the active specie as a catalyst in the transesterification reaction. Therefore, sample BLOS is composed of native oxides of barium and lanthanum and not found very active towards catalysis of transesterification.

3.3.3. Surface morphological analysis

The following SEM images depict the surface morphology of the catalysts prepared via different synthesis routes. Figure 3.3(a) shows the surface morphology of uncalcined catalyst which is composed of clusters of particles acquiring low specific surface area for interaction with reactants during transesterification. Figure 3.3 (b, c, and d) are attributed to SEM images representing surface morphology of prepared catalysts through solid state route, co-precipitation, and citrate route respectively. Among all the four catalysts, BLOA2 particles were separated to the greatest extent as in Figure 3.3 (e). While BLOS particles are not well assorted because of agglomeration at high temperature. BLOA2 sample has more tiny particles as it has insignificant carbonate deposition which is quite prominent in case of BLOA1. This fact is also proved by SEM images (Figure 3.3(d)). The non-agglomerated and well-assorted particles of BLOA2 facile the transesterification reactions by providing high surface area and ultimately show high catalytic activity. Moreover, EDX analysis withstood the

result shown by XRD explaining the stoichiometry of elements in the structural formula (Figure 3.5). The elemental composition of BLOA2 is demonstrated in Figure 3.4 reflecting (%) compositional analysis of all three elements constituting prepared catalyst.

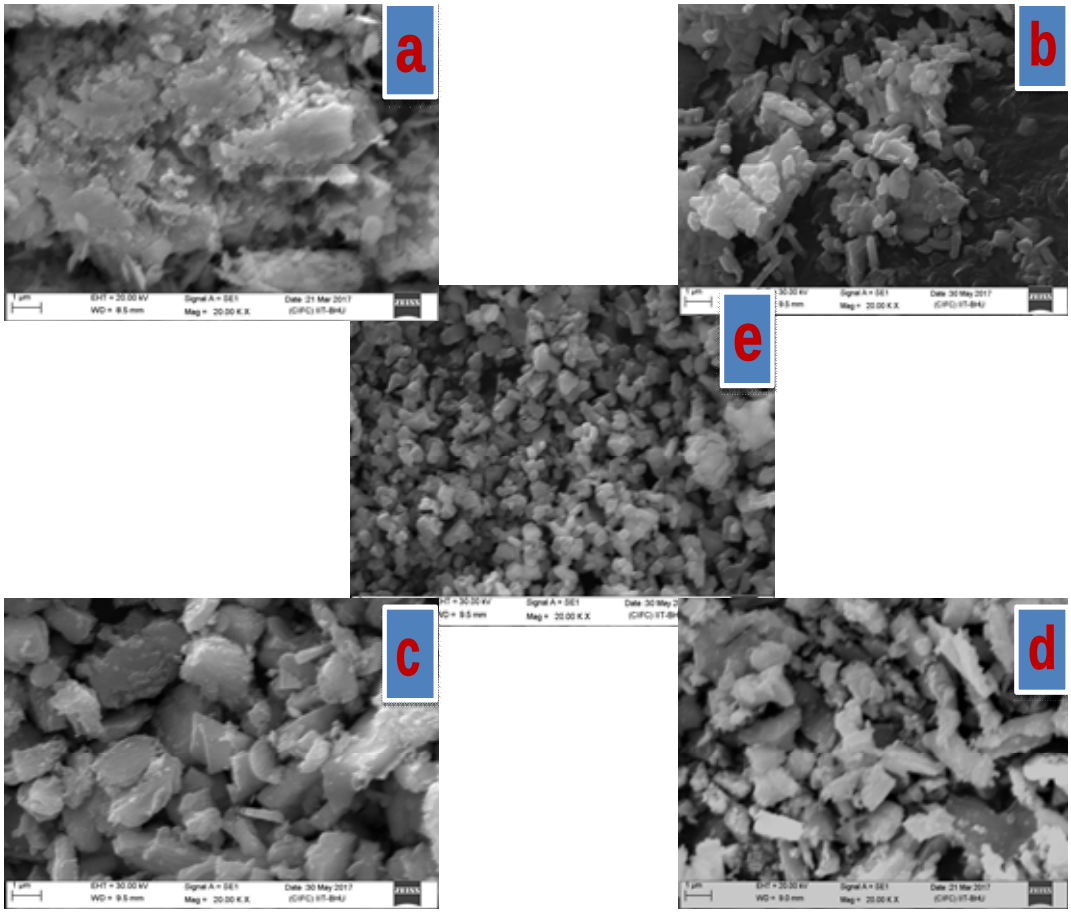

Figure 3.3 SEM image of (a) uncalcined catalyst of BLOA2 and calcined catalysts at 800^{o}C: (b) BLOS, (c) BLOC, (d) BLOA1, and (e) BLOA2.

The catalyst particle size distribution was analyzed by means of Image J software using SEM images in Figure 3.3(e). The particle size in BLOA2 was calculated to be in the range of 0.1-0.6 µm (Figure 3.4).

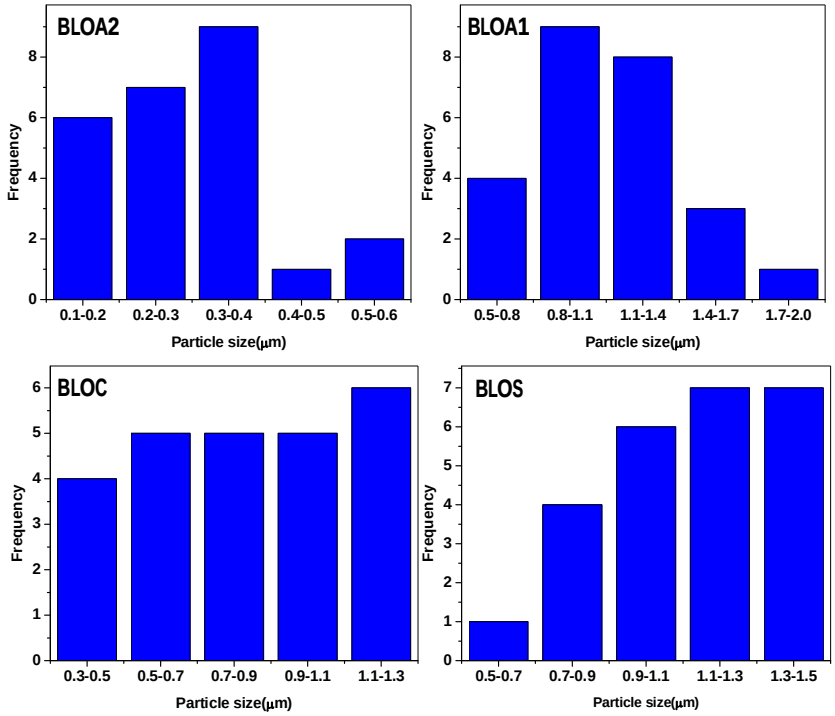

Figure 3.4 Particle size analysis of the catalyst samples using SEM images.

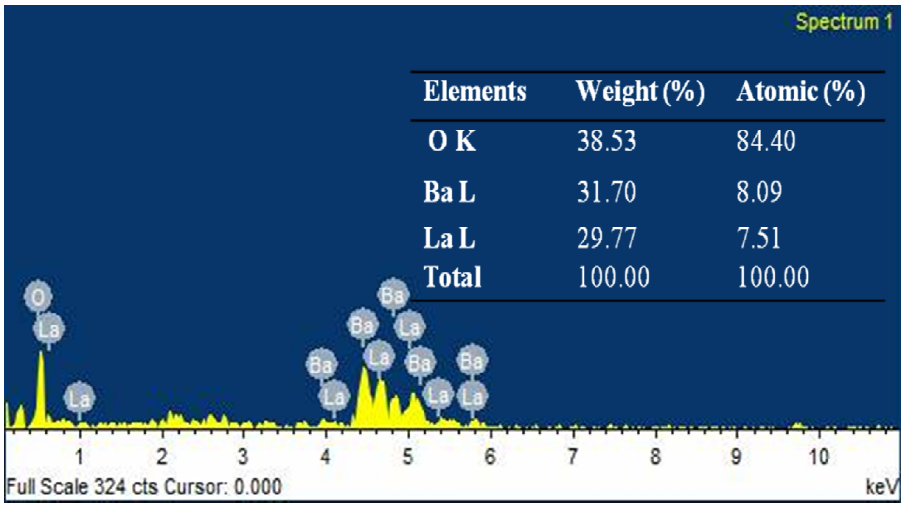

Figure 3.5 EDXS histogram of calcined BLOA2 catalyst.

3.3.4. FT-IR analysis

Infrared analysis of various catalyst samples was recorded to interpret the nature of metal- oxygen bonds in catalyst. Figure 3.6 demonstrates the FT-IR spectra of (a): BLOC, (b): BLOS, (c): BLOA1, (d): BLOA2.

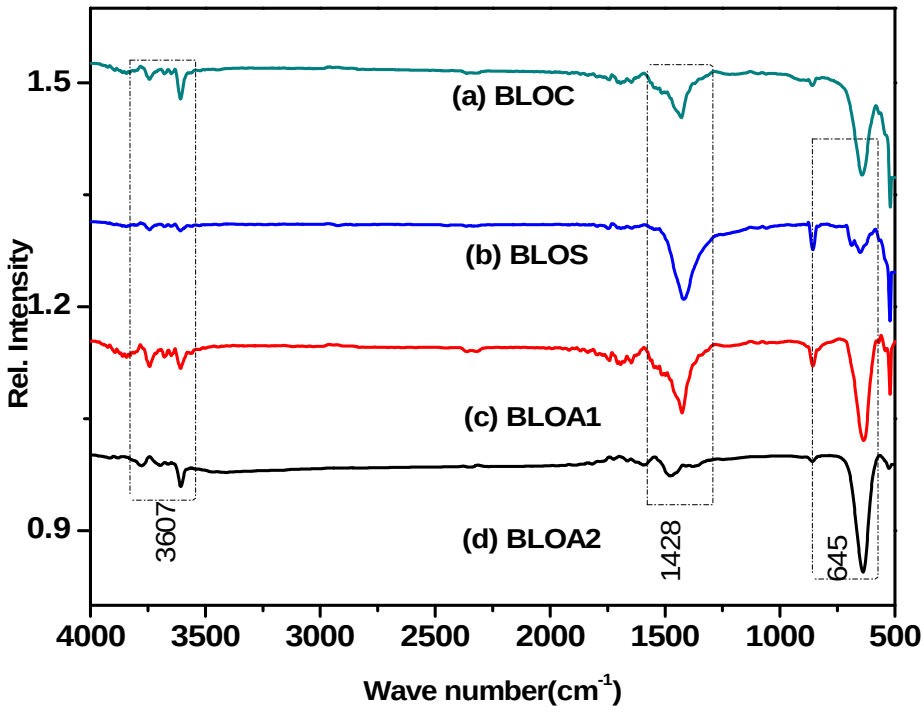

Figure 3.6 FT-IR spectra of (a): BLOC, (b): BLOS, (c): BLOA1, (d): BLOA2.

The FT-IR spectra regarding different samples correspond to stretching frequencies of all major functional groups (different types bonding nature) present in the individual type of above mentioned samples. In case of the solid-state sample (BLOS) as in Figure 3.6(a) the minor intensity peak below 800 cm^{-1} to 550 cm^{-1} corresponds to stretching frequency of individual metal oxide bond (Jonson et al., 1986). The co-precipitation sample (BLOC) has its characteristic peak around 640 cm^{-1} assigned to active metal-oxygen bond. The major broad peak at 1465 cm^{-1} depicts the extent of metal carbonate species which have been trapped during synthesis of catalyst (Taglieri et al., 1999). The sample BLOA1 has shown the same stretching frequency pattern with high-intensity carbonate peak whose presence assuaged catalytic activity. The sample BLOA2 has the capacity to avoid the carbonate formation as nucleation was carried out in the acidic range which avoided carbonate deposition. This finding is

substantiated by FT-IR spectra, Figure 3.6(d), indicating the absence of carbonate peak at 1465 cm^{-1}. Figure 3.6(d) clearly shows a sharp peak at 645 cm^{-1} regarding only characteristics stretching frequency of prepared catalyst having structural formula $Ba_2La_2O_5$ (Sahani and Sharma, 2018). Moreover, peak related to O-H stretching is present in each spectrum which reflects the presence of the trace moisture content in the vicinity of prepared catalyst samples.

3.3.5. BET surface area analysis

Specific surface area (S_{BET}) of all prepared samples was obtained by BET surface area analyzer. From the BET isotherm plot (Figure 3.7), S_{BET} for BLOC, BLOS, BLOA1, and BLOA2 are found to be 6.7m^2/g, 1.3 m^2/g, 13.2 m^2/g and 32.0 m^2/g respectively along with pore size of 9.63nm, 18.15nm, 12.45nm and 6.97nm respectively. The BLOA2 sample has the highest surface area as a result of better dispersion of metal oxides throughout crystal system with insignificant agglomeration. The pore size of individual sample lies in the range of 2-50 nm. Therefore, it eases interaction between prepared mesoporous catalyst and triglyceride (molecular size approx.6nm) (Lee et al., 2014). Since among all prepared sample, BLOA2 seemed to have the highest compatibility for catalysis and facile the diffusion of triglyceride into the pore to react with acyl acceptor generated at the active site on the surface of the catalyst. This ultimately gives highest FAME conversion in the transesterification reaction.

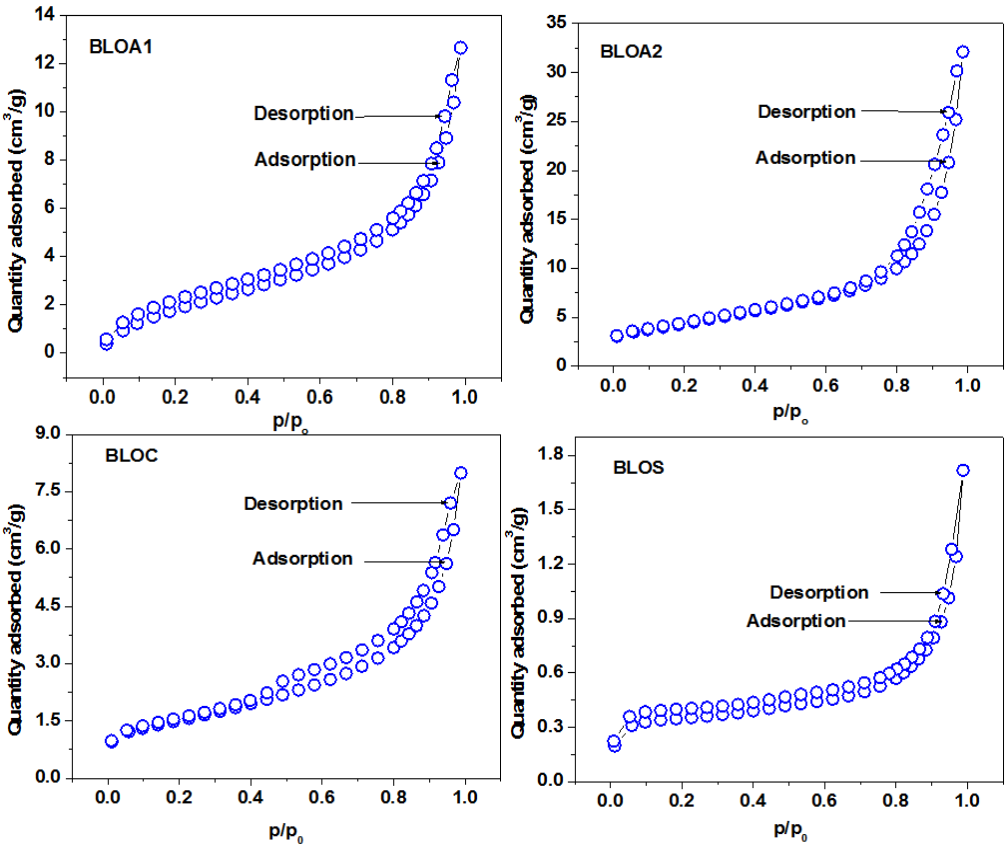

Figure 3.7 N_2 adsorption-desorption isotherm profile of the catalyst samples.

3.3.6. Basicity

The four catalysts had been checked for their basicity. The Lewis basic strength of all four samples was measured using Hammett indicator-benzoic acid titration method. The all four samples had quiet different basic strength depending upon nature of the active sites present on the solid surface. The highest basicity (2.29mmol/g) was observed in BLOA2. This may be attributed to absence of carbonate trapping responsible for diminishing the basic sites on the surface of catalyst (Limaa et al., 2012). Similarly, the BLOA1, BLOC, and BLOS have the basicity of 1.94 mmol/g, 1.84 mmol/g, 1.69 mmol/g, respectively. The lower value of basicity BLOA1 owes to the presence of metal carbonates within crystal lattice which lessens the concentration

of the basic sites. The probable reason for the lowest value of BLOS was least exposed surface area as more of particles are agglomerated, it is also shown by SEM image of BLOS.

3.4. Effect of process variables on FAME conversion

The major factors affecting FAME conversion are listed as catalyst dose (wt%), oil to alcohol molar ratio, temperature, reaction time and stirring speed.

3.4.1. Effect of catalyst synthesis route

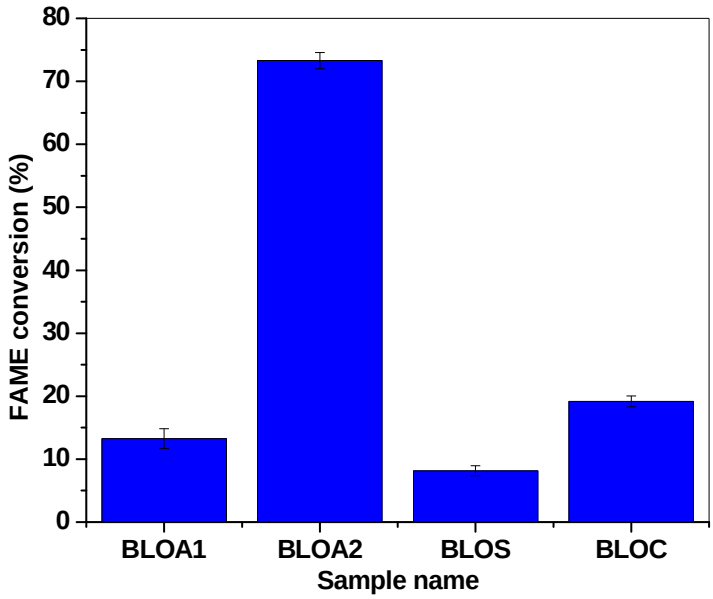

Figure 3.8 Effect of synthesis route on FAME conversion

The catalytic activity of BLOS, BLOC, BLOA1 and BLOA2 was monitored over some randomly adopted reaction conditions (catalyst dose: 1.0 wt%; oil to alcohol molar ratio:: 1:15; reaction temperature: 60˚C; reaction time: 2.5h; stirring speed: 500rpm). Figure 3.8 suggests that amidst four prepared catalyst samples, BLOA2 was proved to be the most suitable for the transesterification reaction and was used as

catalyst for further optimization process. Owing to the greater extent of crystalinity, highest surface area and basicity BLOA2 finds its application as a potential catalyst in present study for biodiesel production. Since BLOA1 has acquired extensive catalytic poisoning due to metal carbonate accommodation, FAME conversion has been drastically reduced to a negligible extent. As expected, similar situation prevails in BLOS and BLOC because of presence of metal carbonate, comparatively lower surface area and basicity.

3.4.2. Effect of oil to methanol molar ratio and catalyst dose

Several steps of optimization were performed including the simultaneous study of catalyst dose and oil to alcohol molar ratio while other process variables were kept as invariant. The catalyst dose was varied from 0.5 to 2.0wt% and oil to methanol molar ratio from 1:6 and 1:22. Figure 3.9(a) constitutes the impact of both catalyst concentration and 'oil: methanol molar ratio' on FAME conversion altogether. It illustrates that FAME conversion starts swiftly with catalyst concentration up to 1.5 wt%. Afterward, it achieved saturation as viscosity mitigates the interphasic mass transfer during transesterification (Balat and Balat, 2010). Since this transesterification comprises of reversible step wise cleavage of triglyceride ester, according to Le Chateleir's principle higher alcohol molar ratios are compulsory to drive the reaction in forward direction (Balat and Balat, 2010; Sahani and Sharma,2018). Here, FAME conversion reached at its maximum at 1:18 oil to methanol molar ratio. Further increment in this ratio as mentioned earlier starts depleting the biodiesel production because glycerol, the side product ensures itself to be assimilated in exorbitant methanol present in the reaction mixture (Banerjee et al., 2019). The highest FAME conversion is offered at 1.5 wt% and 1:18 oil to methanol molar ratio and these

optimized parameters were kept constant for optimization of the remaining process variables.

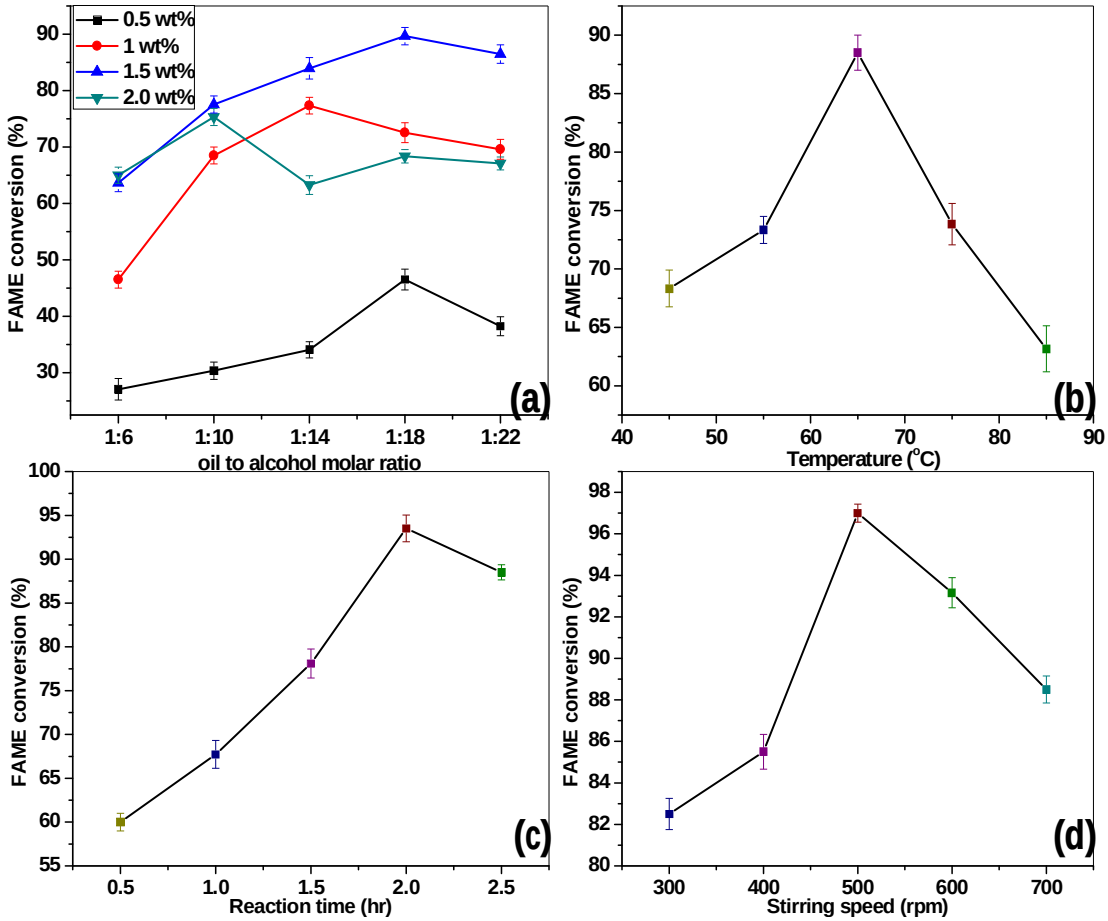

Figure 3.9 Optimization plots (a) Effect of alcohol to oil molar ratio alongwith different catalyst dos (b) Effect of reaction temperature, (c) Effect of reaction time on MOME conversion, (d) Effect of stirring speed.

3.4.3. Effect of reaction temperature

According to kinetic theory, temperature is supposed to be most important factor affecting any chemical reaction. The transesterification reaction has been described as an endothermic reaction in literature (Omar et al., 2011). Le Chatelier's principle states that an increase in reaction temperature favors the reaction in forward direction (Sahani et al., 2019). Therefore, effect of reaction temperature was inspected

to gain impeccable FAME conversion. Figure 3.9(b) clearly indicates that genesis of methyl ester is increasing expeditiously till boiling temperature of methanol under reflux conditions. This may be due to enhancement in sufficient kinetic energy to meet threshold energy barrier for ester conversion. Since, beyond 65˚C methanol starts vaporizing and escapes from reaction mixture reducing its contact with catalyst and triglyceride entity (Madhu et al., 2017). This leads to deterioration in methyl ester formation during transesterification.

3.4.4. Effect of reaction time

The optimization of proper reaction time required for completion of transesterification reaction was assessed at following reaction conditions (catalyst dose: 1.5 wt%; oil to alcohol molar ratio::1:18; reaction temperature: 65˚C; stirring speed: 500rpm). Figure 3.9(c) shows fate of FAME conversion over reaction time. According to Figure 3.9(c), profile reached at its maximum in 2 h, and onwards it got stabilized to some extent of period. But after the prolonged time, it was decreased as hydrolysis of esters along with soap formation accompanies the forward reaction of biodiesel formation (Abbah et al., 2016).

3.4.5. Effect of stirring speed

Heterogeneity of the system makes interaction between reactants more troublesome, so it needs a proper mixing through stirring (Balat and Balat, 2010). For the sake of proper interaction among triphasic system, numerous batches of stirring were conducted with stirring speed ranged between 350 rpm to 850 rpm keeping other parameters at their optimized condition. Initially, MOME conversion is accelerated to its height of saturation with raise in stirring speed to value of 500 rpm shown in Figure

3.9(d). This extent of thorough agitation facilitates better mixing of three different existing phases providing sufficient contact time to react to each other. Further, it tends to cause excessive agitation creating troubles in ester exchange because it reduces enough closeness of reactant species over the surface of the solid catalyst and ultimately mitigates the methyl ester formation.

3.5. Kinetic and thermodynamic studies

As this study belongs to heterogeneous catalysis, slow mass transfer and diffusion reactions sandwiching the fast kinetic reaction (Banerjee et al., 2019) involving the cleavage of triglyceride into acyl species must be taken into account to explain the mechanism. In the present study, the only above mentioned kinetically faster reaction has been interpreted. Assuming all the three subsequent elementary steps followed the same mechanistic order. For kinetics investigation, the experimental data were interpreted regarding reaction time and three different temperatures (318 K, 328 K, and 338 K). Rate constants for each temperature were evaluated using kinetic model, discounting the intermediate steps as in Figure 3.10(a). The resultant plots display reasonable linearity suggesting that the model is suitable for predicting transesterification kinetics data. Moreover, the estimated values of rate constant from Figure 3.10(a) at temperatures 318 K, 328 K and 338 K were found to be 5.2×10^{-3} min^{-1}, 7.3×10^{-3} min^{-1}, 1.1×10^{-2} min^{-1}, respectively. The obtained values were found to increase with raising reaction temperature which supports the results that elevating temperature promotes transesterification process due to enhanced mass transfer effect. The activation energy (E_a) and pre-exponential factor evaluated from Figure 3.10(b) as 34.64kJ mol^{-1} and 2.4×10^{3} min^{-1} respectively. From Figure 3.10(c), values of ΔH° and ΔS° were computed to be 32.12 kJ/mol and -188.33 J/mol, respectively from the linear

plot of Eyring equation i.e. ln (k/T) versus 1/T. The positive value of ΔH^{o} deduced the endothermic nature of transesterification reaction which meant that the external energy supplement was needed for the transformation of reactants to products via in between generation of activated complex (Banerjee et al., 2019) whereas the negative value of ΔS° value was indication of deduction in system randomness. Ultimately, ΔG° values were assessed to be 92.01kJ/mol, 93.89kJ/mol, and 95.78kJ/mol at 318K, 328K, and 338K respectively. The positive ΔG° values asserted the non-spontaneity of the transesterification reaction at any chosen temperature even at most optimized temperature condition (Banerjee et al., 2019). Rather it declared the desirability of a catalyst to make this transesterification reaction feasible to produce biodiesel by renewing path of mechanism with relatively lower activation energy.

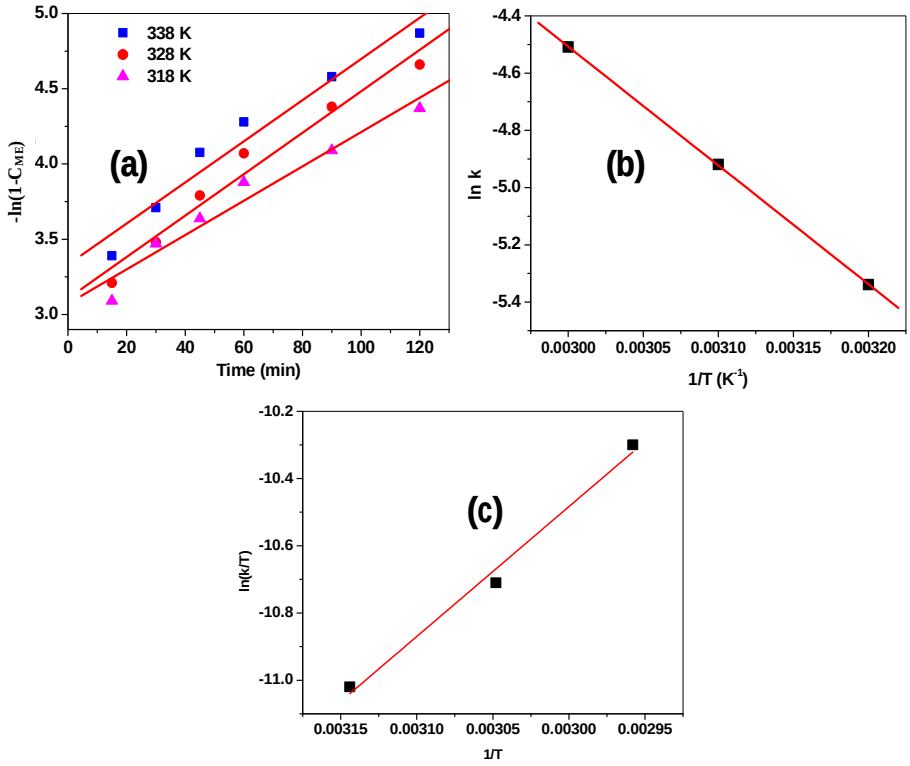

Figure 3.10 (a) $-\ln(1-C_{ME})$ versus reaction time (min) plot at different temperatures, (b)Arrhenius plot lnk versus 1/T (K^{-1}) for transesterification of *Madhuca longifolia* oil by BLOA2, (c) Eyring plot.

3.6. Reusability and leaching studies

After performing the optimization of transesterification, the reusability of catalyst was accomplished to find out recycling capability of the catalyst. Prima facie from Figure 3.11, five times recycling virtue was registered lasting with FAME conversion of 83% in transesterification reaction at following optimum conditions: oil to alcohol molar ratio (1:18), catalyst dose (1.5%), temperature (65^{o}C), stirring speed (500 rpm) and reaction time (2 h). Onward, The FT-IR spectra of the fresh catalyst as well as reused catalyst after five cycles were recorded in Figure 3.11, and plausible comparison between spent catalyst and fresh catalyst was made accordingly on the basis of the peaks appeared in FT-IR spectra. In Figure 3.12, the presence of significant peaks at 2930-2850 cm^{-1} (Singh et al., 2016), confirmed the irreversible attachment of organic residues on the surface of the catalyst which poisons the catalytic activity. This attributed to vibration of asymmetrical stretching of the C-H bond of the methyl group as well as methylene group part of the unsaturated fatty acid moiety. The band around 1740 cm^{-1} (Banerjee et al., 2019) exclusively demonstrated the asymmetric stretching of carbonyl functional group in esters present on the surface and mild intensity peaks around 1150 cm^{-1} showed the stretching vibration of CO group. These additional peaks in FT-IR spectra inferred deactivation of the catalysts due to the impregnation of the ester moiety on the active sites.

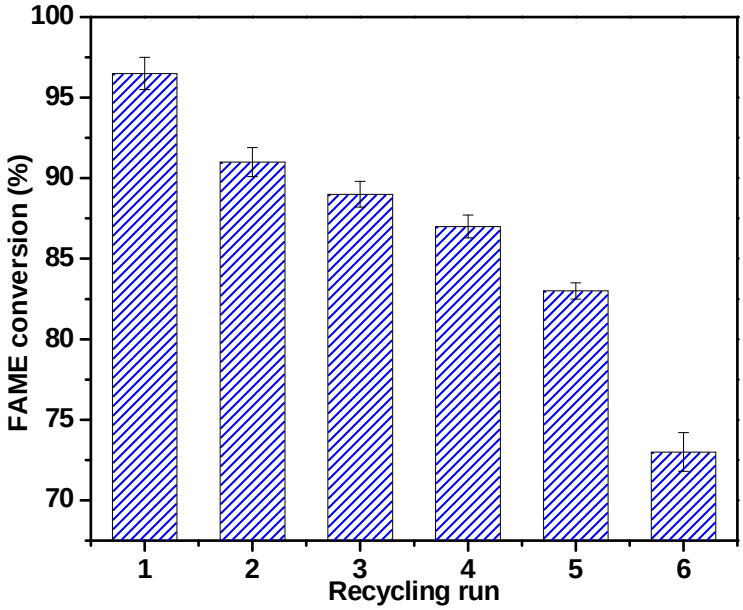

Figure 3.11 Catalyst reusability test profile of BLOA2.

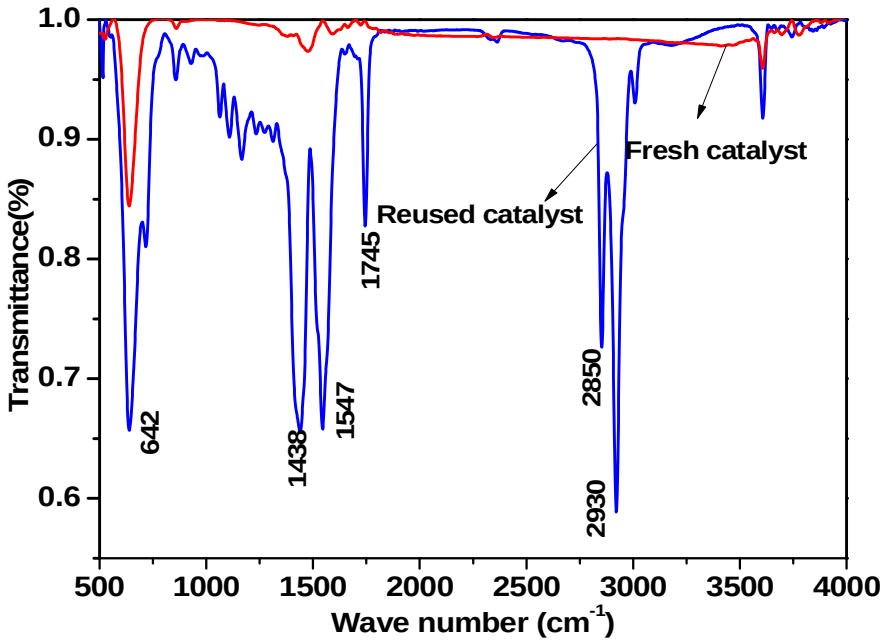

Figure 3.12 ATR FT-IR spectra for comparative study of fresh BLOA2 and used catalyst.

On the basis of the findings from abovementioned kinetic experiments and FT-IR analysis, a tentative mechanism was proposed to understand of transesterification reaction as shown in Figure 3.13. It involves the heterogeneous catalysis on the surface of the solid catalyst.

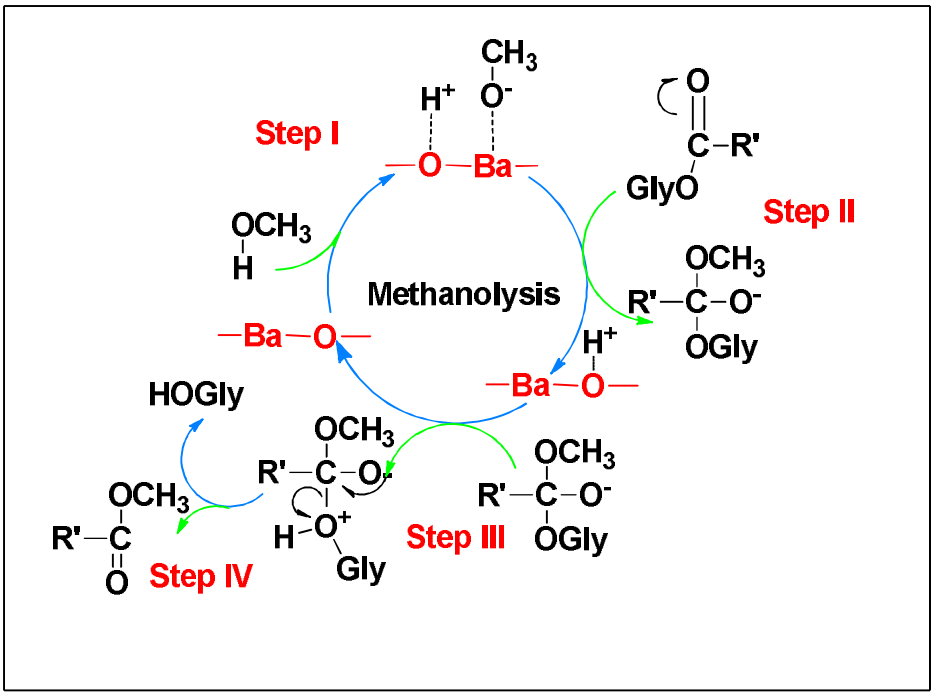

Figure 3.13 An illustration of mechanism of transesterification reaction.

The methanol moiety got adsorbed on the surface of catalyst across Ba-O followed by sharp division of O-H bond in methanol moiety. The kinetically active driving force is the swift generation of acyl acceptors which ultimately receives acyl moiety from triglyceride (Sahani and Sharma, 2018). These acyl acceptors are formed as a result of O-H bond cleavage within methanol molecule. The plausible routes as in Figure 3.13 demonstrated the mechanism responsible for FAME production. Here, catalytic activity laid in the basic strength of Ba-O in BLOA2.

3.7. E-factor and TOF

The greenness approach of this transesterification reaction was estimated by E-factor. The E-factor for this process of biodiesel production was 0.089 which was quite low indicating the greenness of the transesterification reaction. Additionally the potential of Ba-La mixed metal oxide catalyst was evaluated through the turnover frequency (TOF) which quantified the catalytic activity of catalyst undergoing methanolysis followed by surface chemical reaction forming methyl ester. In current study, TOF for transesterification reaction was found as 23×10^{-2} s^{-1}. Almost similar values of TOF were reported in literature for heterogeneous base catalyzed transesterification reaction (Roy et al., 2019).

3.8. Methyl ester characterization

3.8.1. GC-MS

GC-MS analysis of methyl ester was carried out to determine its chemical composition. Gas chromatogram of FAME is shown in Figure 3.14. Mass spectrum was interpreted using NIST database. The components present in the sample were identified and described in Table 3.1. GC-MS profile of FAME depicts five major fatty acids listed in Table 3.1. It infers that feedstock is mainly composed of unsaturated fatty acid constituting more than 75% of total wt%.

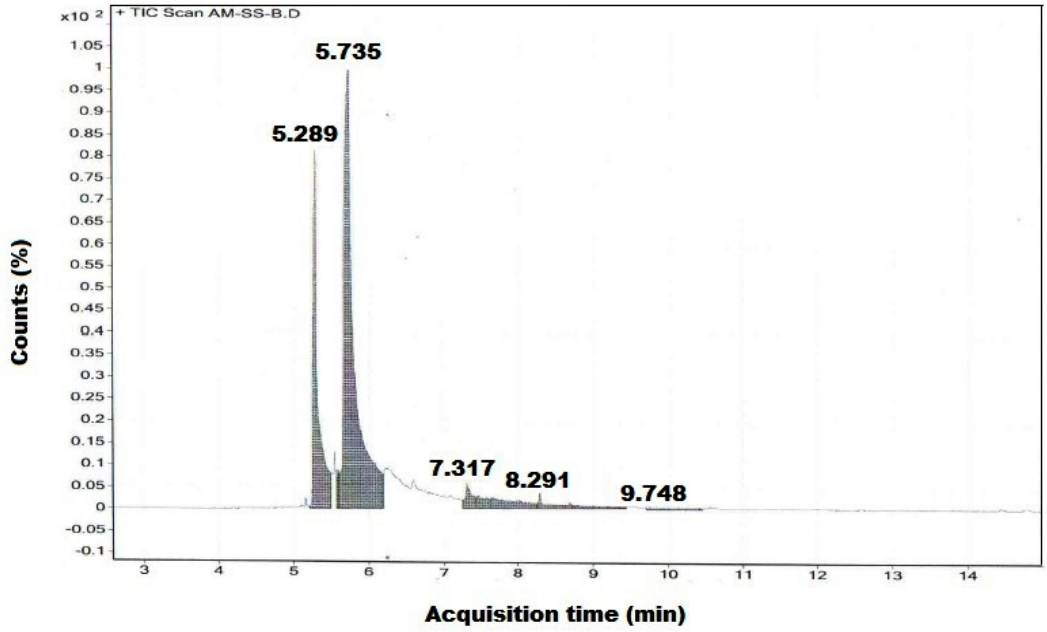

Figure 3.141 GC-MS of methyl ester derived from *Madhuca longifolia* oil.

Table 3.1

Fatty acid composition of methyl ester inferred from GC-MS.

S. No.	Retention time(min)	Corresponding fatty acid	Systematic name	No of Cs: d.b.	Area sum (%)
1	5.289	Palmitic acid	Hexadecanoic acid	C_{16}:0	22.52
2	5.735	Linoleic Acid	9,12-Octadecadienoic	C_{18}:2	64.02
3	7.317	Oleic acid	9-Octadecenoic acid	C_{18}:1	6.27
4	8.291	Palmitoleic acid	9-Hexadecenoic acid	C_{16}:1	3.22
5	9.748	Arachidic acid	Icosanoic acid	C_{20}:0	0.46

3.8.2. ^{1}H-NMR and ^{13}C-NMR

Figure 3.15 manifests ^{1}H-NMR spectra taken corresponding to prepared biodiesel (FAME) at optimum conditions of all concerned process variables during transesterification.

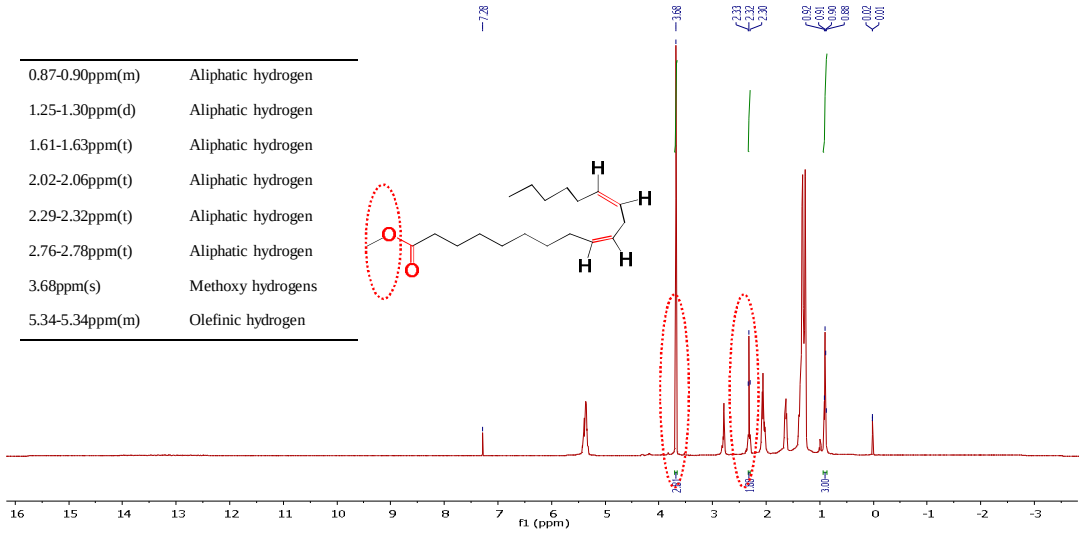

Figure 3.15 ^{1}H- NMR spectra of biodiesel produced at optimized conditions of all process parameters.

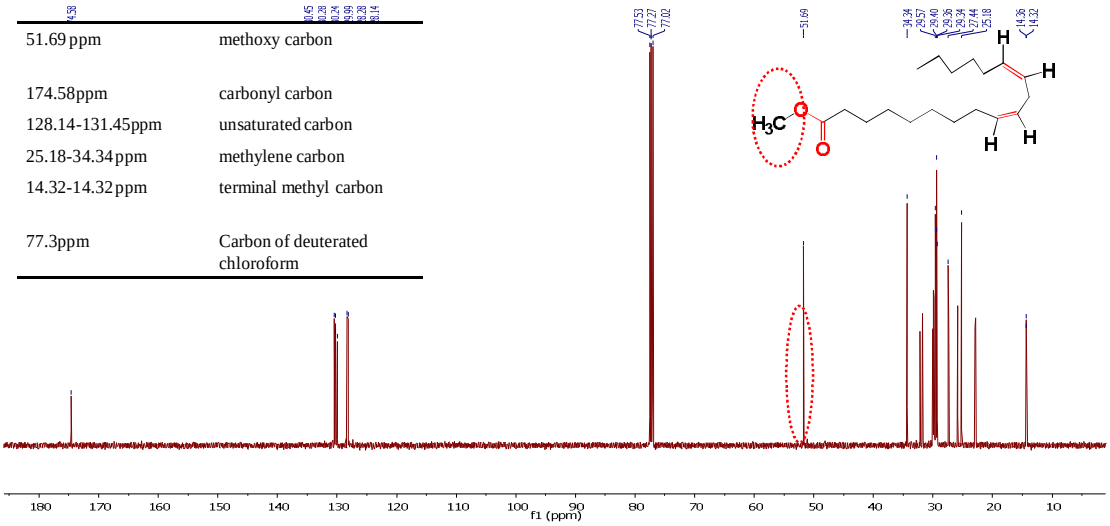

Figure 3.16 ^{13}C-NMR spectra of biodiesel produced at optimized conditions of all process parameters.

The characteristic peak corresponding to methoxy proton was reflected at 3.68 ppm showing the FAME conversion. Additionally, stretching frequency of other peaks regarding carbon backbone of the methyl ester listed in Figure 3.15. Figure 3.16 manifests ^{13}C-NMR of prepared FAME derived from *Madhuca longifolia* oil feedstock which reflects the characteristic signal at 51.69 ppm corresponding to methoxy carbon. Notwithstanding, the absence of NMR signal at 68.8 attributing to methylene carbon confirmed the methyl ester conversion.

3.8.3. ATR FT-IR

The produced methyl linoleate, biodiesel was analyzed by FT-IR analysis for its functional group analysis in Figure 3.17.

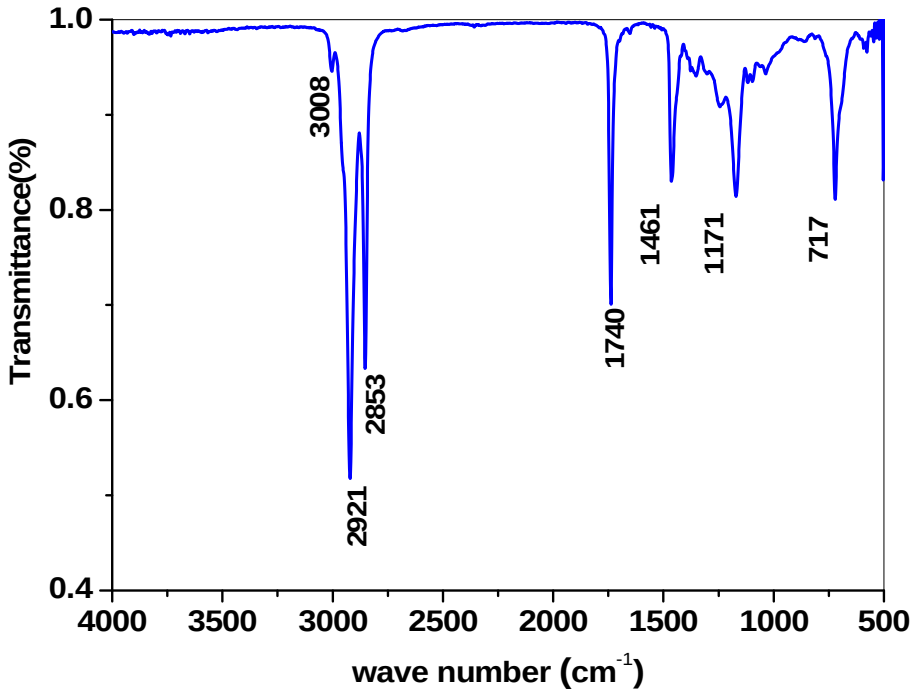

Figure 3.17 ATR FT-IR spectra for comparative study of fresh BLOA2 and used catalyst.

Basically, methyl ester is characterized by the high intensity peak near 1740 cm^{-1} owing to C=O stretching frequency. The position of carbonyl band in FT-IR spectra is quite sensitive to its adjacent functional groups (Tariq et al., 2011). In Figure 3.17, it was seen that the carbonyl stretching peak was transitioned from 1748 cm^{-1} in mahua oil to 1740 cm^{-1} in FAME (Devi et al., 2015). The sharp peak at 3008 cm^{-1} was regarded to olefinic C-H stretching (-HC=CH-) in FAME while the peak appeared at 2921 cm^{-1} owed to asymmetric C-H stretching in -CH_3 and peak observed at 2853 cm^{-1} was attributable to -CH- stretching in O-CH_3 (Tariq et al., 2011). The asymmetric and symmetric vibrations corresponding to CH_3 deformation were noticed near 1461 cm^{-1} and 1362 cm^{-1} respectively. The noticeable peaks at 874 $cm^{-1}$and 585 cm^{-1} were related to -C-O-C- stretching and bending vibrations (Tariq et al., 2011). The peak at 717 cm^{-1} corresponded to CH_2 bending vibrations, whereas the peak at 921 cm^{-1} presented C-H bending vibration from substituted -C=C- part. Moreover, the strong and broad peaks in the range of 1000 cm^{-1} to 1200 cm^{-1} showed the stretching of acyl (-C=O). Ultimately, this typical FT-IR spectrum of transesterified mahua oil vindicated the presence of FAME.

3.8.4. Investigation of physicochemical properties of methyl ester

The compatibility FAME derived from *Madhuca longifolia* oil for CI engine over conventional fuel was figured out by assuring the quality of produced biodiesel after physicochemical analysis. Table 3.2 shows the comparative study of physicochemical properties regarding both the feedstock as well as FAME. The study of physicochemical properties has included the important properties viz. average calorific value, cetane number density, fire point, flash point, kinematic viscosity and saponification number. The FFA value of crude *Madhuca longifolia* oil was found to be

14 mg of KOH per gm, whereas that of methyl ester was 0.65 mg of KOH per gm. Saponification value of FAME was curtailed to 151 mg of KOH per gm within ASTM standard range. Transesterification lessened density value from 0.871g/cm^3 to 0.863g/cm^3. Calorific value and cetane number of FAME was assessed to be 36.95 MJ/kg and 50 respectively. The fire point and the flash point of FAME were determined to be 143˚C and 132˚C respectively. The report corresponding to each property has been found to be in good agreement with those prescribed by ASTM standards. This enables FAME a suitable fuel alternative which mocks the petrodiesel for aforementioned properties.

Table 3.2

An illustration of physicochemical properties of FAME produced from *Madhuca longifolia* oil.

Properties	**Unit**	***Madhuca longifolia* oil**	**FAME**	**ASTM standards**
Acid value	mg KOH/g	13.4	0.75	D664
color	-	Yellowish red	Light yellowish	Yellowish
Calorific value	(MJ/kg)	39.50	36.95	D4809
Copper strip corrosion	-	1a	1a	D130
Cetane no.	-	43	50	D 613
Density (at 15˚C)	g/cm^3	0.871	0.863	D1298
Flash point	˚C	215	132	D93
Fire point	˚C	255	143	D93
Kinematic viscosity(at 40˚C)	mm^2/s	23.7	5.9	D445

3.9. Conclusions

In the present study, FAME was synthesized from *Madhuca longifolia* oil in two subsequent steps, i.e., esterification followed by the catalysed transesterification reaction. Four samples of novel catalyst (BLOA1, BLOA2, BLOC, and BLOS) were prepared by four different synthesis protocols, i.e., sol-gel auto-combustion (BLOA1 and BLOA2), co-precipitation (BLOC) and solid-state route (BLOS). Co-precipitation route and solid route did not prove to be significant enough to produce the efficient catalyst. BLOA1 was also not the suitable candidate as a catalyst for transesterification as surface passivation was observed with carbonate adsorption. BLOA2 was perceived to be most catalytically active with the highest purity and high crystallinity in the absence of carbonate species. Hence BLOA2 was utilized as a novel heterogeneous basic catalyst. The MOME was characterized by ^{1}H-NMR for FAME conversion. All important process variables were optimized to obtain maximum 97.2±0.5% FAME conversion as catalyst concentration (1.5wt %), oil to alcohol molar ratio (1:18), temperature (65˚C), reaction time (2h), and stirring speed (500 rpm). The reaction mechanism followed first-order kinetics. The activation energy (E_A) was found to be 34.64kJ/mol and the frequency factor (A) was found to be 2.4×10^{3} min^{-1}. The thermodynamic functions such as ΔH°, ΔS°, and ΔG° were also calculated as 32.12 kJ/mol, -188.33 J/mol, and 95.78 kJ/mol at 65˚C. The positive value of Gibbs free energy (ΔG°) suggested the transesterification reaction as non-spontaneous or external force driven reaction which validates the need of heterogeneous catalysis. The E-factor and turn over frequency (TOF) were also determined and found to be 0.089 and $23\times10^{-2}s^{-1}$. The physicochemical properties of the synthesized biodiesel were measured according to ASTM D 6751 and found to be within the permissible range.